

Document Version

Final published version

Licence

CC BY-NC-ND

Citation (APA)

Grasso, F., Bismuth, E., Burchard, H., Defontaine, S., Kösters, F., Lafite, R., Reese, L., Sottolichio, A., van Kessel, T., Vanlede, J., van Maren, D. S., Walther, R., & Zorndt, A. (2026). Relating estuarine turbidity maxima to tide and river conditions. *Scientific Reports*, 16(1), Article 3096. <https://doi.org/10.1038/s41598-025-32950-7>

Important note

To cite this publication, please use the final published version (if applicable). Please check the document version above.

Copyright

In case the licence states “Dutch Copyright Act (Article 25fa)”, this publication was made available Green Open Access via the TU Delft Institutional Repository pursuant to Dutch Copyright Act (Article 25fa, the Taverne amendment). This provision does not affect copyright ownership. Unless copyright is transferred by contract or statute, it remains with the copyright holder.

Sharing and reuse

Other than for strictly personal use, it is not permitted to download, forward or distribute the text or part of it, without the consent of the author(s) and/or copyright holder(s), unless the work is under an open content license such as Creative Commons.

Takedown policy

Please contact us and provide details if you believe this document breaches copyrights. We will remove access to the work immediately and investigate your claim.



OPEN Relating estuarine turbidity maxima to tide and river conditions

Florent Grasso^{1✉}, Elliott Bismuth¹, Hans Burchard², Sophie Defontaine¹, Frank Kösters³, Robert Lafite⁴, Lloyd Reese², Aldo Sottolichio⁵, Thijs van Kessel⁶, Joris Vanlede⁷, Dirk Sebastian van Maren⁸, Régis Walther⁹ & Anna Zorndt³

Tidal rivers and estuaries may experience high levels of suspended particulate matter (SPM), which impacts water quality and ecosystem functioning. The processes controlling the development of estuarine turbidity maxima (ETM) are fairly well understood. However, predicting the maximum SPM concentration in an estuary based on aggregated parameters (estuarine dimensions, river discharge, tidal range) remains, up to now, impossible without extensive in-situ measurements and/or numerical models. This study introduces an approach that links the strength of the ETM to the tidal, river, and morphological characteristics of a system. Using in-situ data from contrasting meso- to macro-tidal estuaries, we found a consistent pattern of maximum SPM concentrations within a two-dimensional parameter space. The resulting turbidity diagram reveals a high SPM hotspot in estuaries with specific forcing conditions, corresponding to intermediate relative tidal amplitudes and freshwater Froude numbers. This multi-site research advances our predictions of ETM intensity in tide-dominated estuaries, offering a straightforward method to explore potential turbidity trajectories under various human pressures.

Suspended particulate matter (SPM) is a major component of estuarine ecosystems. Marine and river sediment sources provide significant supplies for estuaries, helping to mitigate the potential impacts of mean sea-level rise¹, while internal sediment fluxes reshape estuarine morphology and bed substrate^{2–4}. Additionally, SPM plays a key role in regulating the transfer of nutrients, contaminants, and pollutants along the land-sea continuum⁵. However, high concentrations of SPM (SPMCs) can negatively impact estuarine ecological functions: (i) by increasing water turbidity, which reduces light penetration and limits primary production by phytoplankton⁶; (ii) by decreasing dissolved oxygen levels due to higher organic matter content^{7,8}; and (iii) by impairing the biofiltration and respiratory abilities of benthic and pelagic organisms^{9,10}.

The maximum SPMC can significantly vary between estuaries^{11,12}. It depends on forcing conditions (e.g., river discharge, tides, waves, and wind), system morphology, sediment availability, and management strategies (e.g., maintenance dredging and water supply regulations). Estuaries can evolve from low to high turbidity levels under the pressure of human-induced changes, such as estuary deepening and narrowing, with surface SPMs shifting from $O(0.1 \text{ g/l})$ to $O(10 \text{ g/l})$ ^{13–15}. Conversely, the SPMC can decrease by around half after the construction of estuarine dams, due to the loss of tidal prism and weakening of tidal currents^{16–19}. Over the past few decades, advances in the understanding of estuarine sediment dynamics have improved knowledge of the processes responsible for sediment trapping in tidal estuaries^{20–24}. The formation of an estuarine turbidity maximum (ETM) can be summarised as the convergence of seaward river-induced sediment transport and up-estuary sediment transport resulting from baroclinic circulation and tidal asymmetries^{25,26}. Fine sediments trapped within the estuary can then be resuspended by tidal currents, increasing the water column turbidity. Still, quantifying the ETM intensity is challenging without conducting expensive in-situ measurements or deploying complex numerical models, due to the non-linear interactions between physical processes.

Various studies have attempted to relate SPMC to estuarine parameters using simplified formulas. Based on a multi-estuary study, Uncles, et al.¹¹ found that the largest SPMs occurred in the longest estuaries with the greatest tidal ranges. However, this relationship mainly results from larger tidal currents in long, energetic estuaries, which may lead to significant sediment resuspension. Still, it does not explain why the SPMC in meso-tidal and medium-sized estuaries (e.g., the Ems Estuary¹⁴) can surpass that of macro-tidal and long estuaries (e.g.,

¹Centre de Bretagne, Ifremer – DYNECO/DHYSED, F-29280 Plouzané, CS 10070, France. ²Leibniz Institute for Baltic Sea Research Warnemünde, Rostock, Germany. ³Federal Waterways Engineering and Research Institute, BAW, 22559 Hamburg, Germany. ⁴Univ Rouen Normandie, UNICAEN, CNRS, M2C UMR 6143, F-76000 Rouen, France. ⁵Univ Bordeaux, CNRS, Bordeaux INP, EPOC, UMR 5805, F-33600 Pessac, France. ⁶Department of Ecosystems and Sediment Dynamics, Deltares, Delft, Netherlands. ⁷Flanders Hydraulics, Berchemlei 115, 2140 Antwerp, Belgium. ⁸Faculty of Civil Engineering and Geosciences, Delft University of Technology, 2628 Delft, CN, The Netherlands. ⁹ARTELIA, 6 rue de Lorraine, F-38130 Echirolles, France. ✉email: florent.grasso@ifremer.fr

the Seine Estuary²⁷. In another comparative study, Jay, et al.¹² observed a link between the trapping efficiency of an estuary—the ratio of its maximum SPMC to the dominant (fluvial or marine) sediment source concentration—and the supply number, calculated as the river-to-tidal velocity ratio (U_R/U_T). This method provides a simplified way to describe the ETM; however, similar trapping efficiencies appeared for very different supply number values (e.g., comparing the Ems, Seine, and Gironde estuaries). This suggests that trapping efficiency does not consistently and solely depend on the supply number. A potential reason for the differences observed in these previous parametric studies is the limited consideration of tidal asymmetry at the system scale²⁸.

Geyer and MacCready²⁹ developed a two-dimensional parameter space to characterise estuarine circulation as a function of a freshwater Froude number and mixing number. In this study, we develop a more empirical approach to explore a parameter space for estuarine sediment dynamics, including parameters related to ETM formation: a Froude number (quantifying estuarine circulation and fluvial flushing) and a number representing tidal asymmetry. We collect readily available in-situ data from 7 contrasting tidal estuaries to derive a parameter space for maximum SPMC. This approach offers a heuristic depiction of the forcing conditions leading to high turbidity levels. Therefore, we highlight the presence of a high-turbidity hotspot associated with specific tidal, river, and morphological conditions. Additionally, this study offers a framework for investigating the potential impacts of human-induced pressures (e.g., estuary deepening) on turbidity trajectories in tide-dominated estuaries.

Results

Learning from extensively investigated tidal estuaries

The study draws on knowledge from hydrodynamics and sediment dynamics in seven main estuaries: the Elbe³⁰, Scheldt³¹, Weser³², Seine³³, Loire³⁴, Gironde³⁵, and Ems¹⁴ (Fig. 1). These semidiurnal meso- to macro-tidal estuaries (median tidal range $TR_{p50} = 2.7\text{--}5.4$ m; Table 1) vary in length from 47 to 169 km, with their relative length representing mid- to long estuarine configurations ($L_{est}/L_{tide} = 0.8\text{--}2.1$, with L_{est} the estuary length and L_{tide} the tidal wave length; see the Method section for more details). The mean river discharges range from 61 to 935 m³/s, and the maximum SPMC at the surface indicates intermediate to highly turbid conditions (95th percentile $SPMC_{p95} = 0.3\text{--}6.1$ g/l). According to the estuarine classification proposed by Geyer and MacCready²⁹, these estuaries range from stratified to well-mixed conditions (Figure S1).

The longitudinal analysis of estuarine dynamics reveals contrasting systems (Fig. 2). Tidal evolution encompasses hyposynchronous to hypersynchronous conditions^{36,37}, resulting in different tidal distortion (a/h) along estuaries (with $a = TR/2$ the tidal amplitude and h the water depth) (Fig. 2c). An increase in a/h results in more frictional losses, leading to tidal deformation, and generates flood-dominant tides in both short tidal basins²⁸ and longer funnel-shaped estuaries³⁸. The horizontal salinity gradients (dS/dx) also substantially differ between estuaries, with the largest values occurring in estuaries characterised by large freshwater Froude numbers (Fr_f), such as the Seine and Loire estuaries (Fig. 2d to f). Additionally, vertical gradients in salinity and SPMC (Fig. 2e and g), resulting from the balance between stratification and mixing, differ as illustrated with the well-mixed Gironde Estuary and the strongly stratified Seine Estuary. Also note that the along-estuary SPMC distribution can strongly depend on tidal and river discharge changes, such as the Loire Estuary, or be more uniform, such as the Weser Estuary (Fig. 2g). These systems have been thoroughly studied at the local level over the past decades^{39–45}; here, we use existing datasets to infer the macro-behaviour of their ETMs.

A parameter space for estuarine turbidity maximum

Parameter spaces for estuarine turbidity have already been proposed, for example by Uncles, et al.¹¹ for the maximum SPMC or by Jay, et al.¹² for the trapping efficiency. However, the inadequacy of the proposed approximations with our estuary dataset prompted the need for further investigation (Figures S2 and S3). Therefore, using one-year in-situ measurements from the seven main estuaries, we investigated the distribution of the estuarine turbidity maximum as a function of two parameters (Fig. 3): the freshwater Froude number $Fr_{s,m}$ and the integrated relative tidal amplitude a_0/h_m . Herein, a_0/h_m serves as an easily accessible proxy for the tidal deformation at the system's scale, and the resulting tidal non-linearities^{28,38}, whereas $Fr_{s,m}$ represents baroclinic circulation and flushing^{46,47} (see computation details in the Method section). For each tidal cycle at the most turbid station of each estuary, the highest quartile of surface SPMC (i.e., 75th percentile) is associated with an a_0/h_m - $Fr_{s,m}$ couple (Fig. 3a) and is then interpolated through the parameter space (Fig. 3b).

Estuary data covered a broad area within the parameter space, with some overlap. However, results showed a remarkably consistent distribution of $SPMC_s$ when intercomparing the seven estuaries, revealing a high-turbidity hotspot around $a_0/h_m \approx 0.2\text{--}0.3$ and $Fr_{s,m} \approx 0.01\text{--}0.02$. This illustrates that estuarine turbidity increases under specific river and tidal forcing and supports the idea that the current turbidity diagram provides a relevant parameter space for capturing this trend. The estuarine trapping efficiency ($SPMC_s/SPMC_{ref}$)¹², where $SPMC_{ref}$ is the dominant (fluvial or marine) sediment source concentration (Table 1), exhibits a similar distribution within this parameter space (Fig. 3c and d). It emphasises that surface SPMC in the ETM area can surpass the sediment source concentration by one or two orders of magnitude.

Complementary test estuaries

The ETM parameter space was subsequently verified with five test estuaries: the Vilaine⁴⁸, the Charente⁴⁹, the Hudson⁵⁰, and the Loire in 1900 and 2000¹⁵. Input variables (a_0 , Q_0 , h_m , and w_m) and the resulting SPMC ($SPMC_s$) were obtained from available literature (Table 1; see details in the Data Availability section). These estuarine forcings represent conditions with a large tidal range and low river discharge, when the ETM is potentially the most intense (open circles in Fig. 3b).

The hyper-turbid Charente Estuary corresponds to conditions of the high-turbidity hotspot ($a_0/h_m \approx 0.3$ and $Fr_{s,m} \approx 0.02$). Contrastingly, the short Vilaine Estuary and long Hudson Estuary are located in the

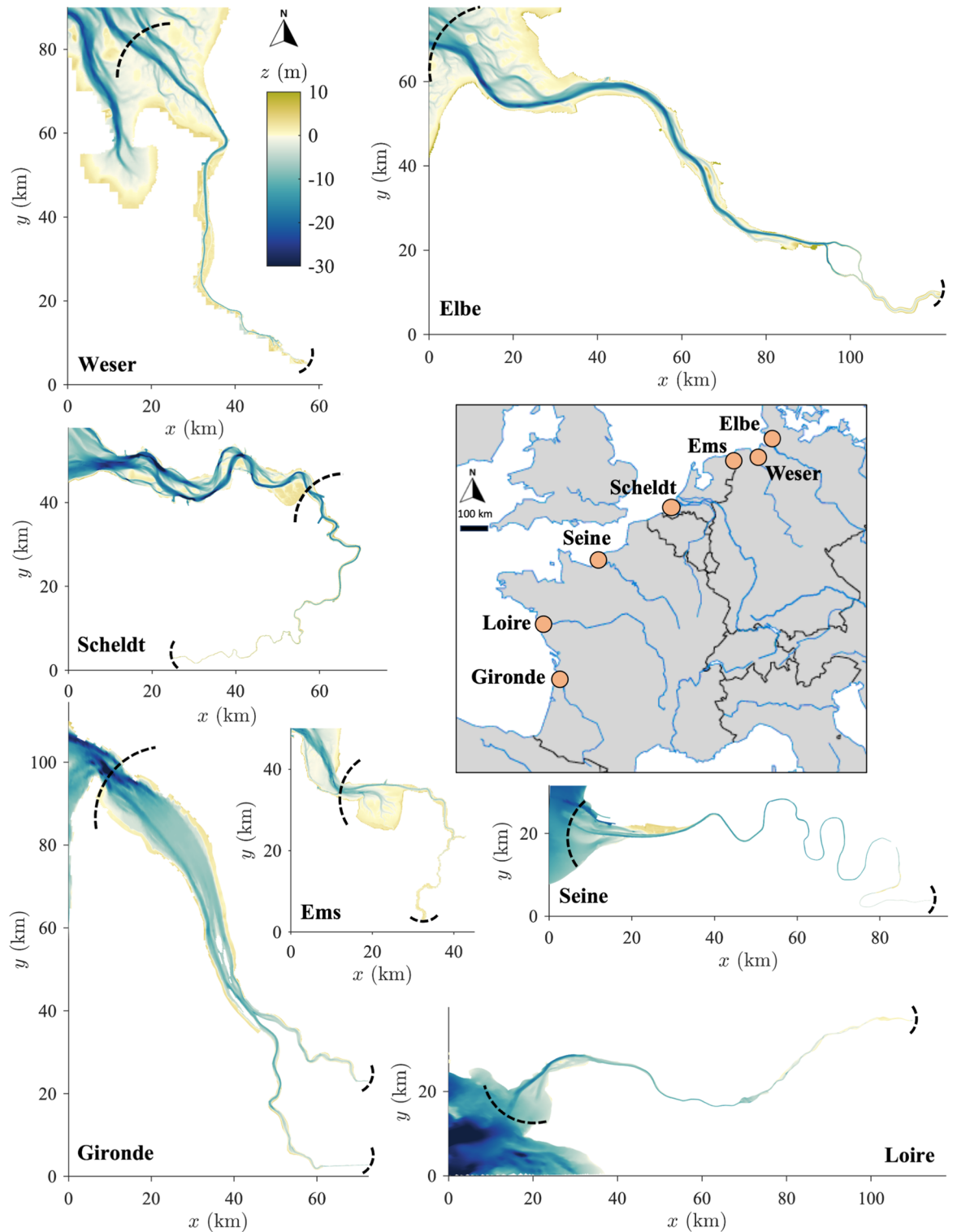


Fig. 1. Morphologies of the seven main estuaries. Map of the estuary locations in Northwestern Europe and their respective elevation z relative to mean sea level. Black dashed lines represent seaward and landward estuary boundaries.

lower turbidity regions of the diagram, consistent with their lower turbidity levels. Note that their limited ETM intensity results either from tidal distortion that is too weak or too strong. In addition, the configurations of the Loire, which differ only by the deeper thalweg depth in 2000 ($h_m = 9.6$ and 5 m, respectively; Table 1), effectively demonstrate the SPMC increase associated with estuary deepening¹⁵. Thus, these test

		Estuary length (L_{est}) [km]	Relative length (L_{est}/L_{tide}) [-]	Depth (h_m) [m]	Width (w_m) [m]	Seaward tidal range (TR_0) [m]	River discharge (Q_0) [m ³ /s]	Surface SPMC ($SPMC_s$) [g/l]	Reference SPMC ($SPMC_{ref}$) [g/l]	River sediment supply [Mt/y]
Main estuaries	Elbe (2013)	158	1.7	17.8	2007	2.8 (1.9–3.3)	935 (399–2263)	0.09 (0.02–0.29)	0.020	0.7
	Scheldt (2006)	89	1.3	10.2	396	3.8 (2.7–4.7)	82 (42–218)	0.19 (0.09–0.37)	0.039	0.1
	Weser (2016)	89	1.1	13.1	487	2.7 (2.0–3.3)	207 (101–683)	0.36 (0.18–0.53)	0.023	0.4
	Seine (2016)	169	2.1	13.1	315	5.4 (3.3–7.3)	445 (286–1312)	0.28 (0.04–1.07)	0.028	0.8
	Loire (2018)	111	1.6	8.9	410	3.6 (1.8–5.1)	644 (147–2507)	0.20 (0.04–2.91)	0.027	1.6
	Gironde (2015)	125	1.8	8.3	1552	3.3 (1.9–4.7)	382 (154–1633)	0.77 (0.08–5.13)	0.024	0.9
	Ems (2005)	47	0.8	5.9	227	3.1 (2.4–3.6)	61 (32–156)	2.37 (0.16–6.08)	0.050	0
Test estuaries	Vilaine (2007)	12	0.2	5.0	1578	4	30	0.20	N.A.	N.A.
	Charente (2012)	55	0.9	6.9	50	4	10	4.00	N.A.	N.A.
	Loire (1900)	104	1.5	5.0	400	4.3	160	0.50	N.A.	N.A.
	Loire (2000)	95	1.4	9.6	400	4.3	160	2.50	N.A.	N.A.
	Hudson (1999)	187	2.2	14.4	500	1.5	200	0.10	N.A.	N.A.

Table 1. Yearly-averaged hydrodynamic and sediment parameters for the main estuaries and the test estuaries. Numbers represent median values, and parentheses contain the 5th and 95th percentiles. SPMC data are selected for each estuary at the station measuring the highest SPMC along the estuary over a year. Based on the literature, the dominant source of SPMC ($SPMC_{ref}$) is defined at the riverside for all the estuaries, except the Ems and the Weser, where the marine source is dominant. Data are retrieved from in-situ measurements and numerical simulations. See details on dataset references in the data availability section. ‘N.A.’ designates unavailable data.

estuaries confirmed the relevance of the parameter space to globally characterise the ETM intensity based on easily obtained variables.

Discussion

High-turbidity levels under specific tide and river conditions

The combination of field observations on the seven main estuaries and the five test estuaries provided a relevant distribution of maximum SPMC and sediment trapping efficiency in the proposed parameter space. A high-turbidity hotspot was obtained for intermediate relative tidal amplitudes and freshwater Froude numbers. These optimum conditions for reaching high SPMC can be related to the concurrence of sediment convergence and resuspension²⁶. On one hand, the simplified freshwater Froude number acts as a proxy for the baroclinic circulation^{46,51}, which enhances sediment trapping within the estuary. However, an excessively large $Fr_{s,m}$ (i.e., a large U_R) can lead to a dominant river-induced sediment export, reducing the sediment trapping efficiency¹², which explains the decreasing turbidity observed at large $Fr_{s,m}$. On the other hand, the relative tidal amplitude not only represents the tidal asymmetries and the associated tidal pumping^{28,52}, but can also be seen as a proxy of the tidal velocity⁴⁷. Therefore, a_0/h_m relates to both sediment trapping and resuspension, and should increase with the SPMC⁵³. Nonetheless, the decrease in SPMC observed with large a_0/h_m is consistent with highly energetic tidal estuaries, where sediment trapping is reduced due to tidal sediment dispersion^{11,22,54}.

These observations illustrate the systems’ capacities to trap and resuspend sediment under particular tidal, river, and morphological conditions. However, human interventions, such as land reclamation, dam construction, maintenance dredging activities, and sediment removal, can also influence actual turbidity levels by altering the available sediment pool. Additionally, the ETM is sensitive to local setbacks, such as the presence of pits and intertidal areas, which may act as sediment sinks or sources and impact the SPMC⁵⁵.

A simplification of the complex reality

The proposed ETM parameter space reveals a surprisingly consistent pattern in SPMC, despite our considerable simplification of the complexity of estuarine dynamics. Firstly, lateral subtidal and intertidal morphological features influence estuarine dynamics⁵⁶, whereas we use an average estuary width and thalweg depth. Secondly, investigating surface turbidity allows for a broader analysis of available estuarine datasets (which are often collected near-surface), but ignores vertical gradients associated with local stratification, mixing, and flocculation processes^{57,58}. Thirdly, the current ETM parameter space does not account for wind and wave forcing. Although their influence on ETM is second-order in macro-tidal environments³³, they can be significant in low-tidal-

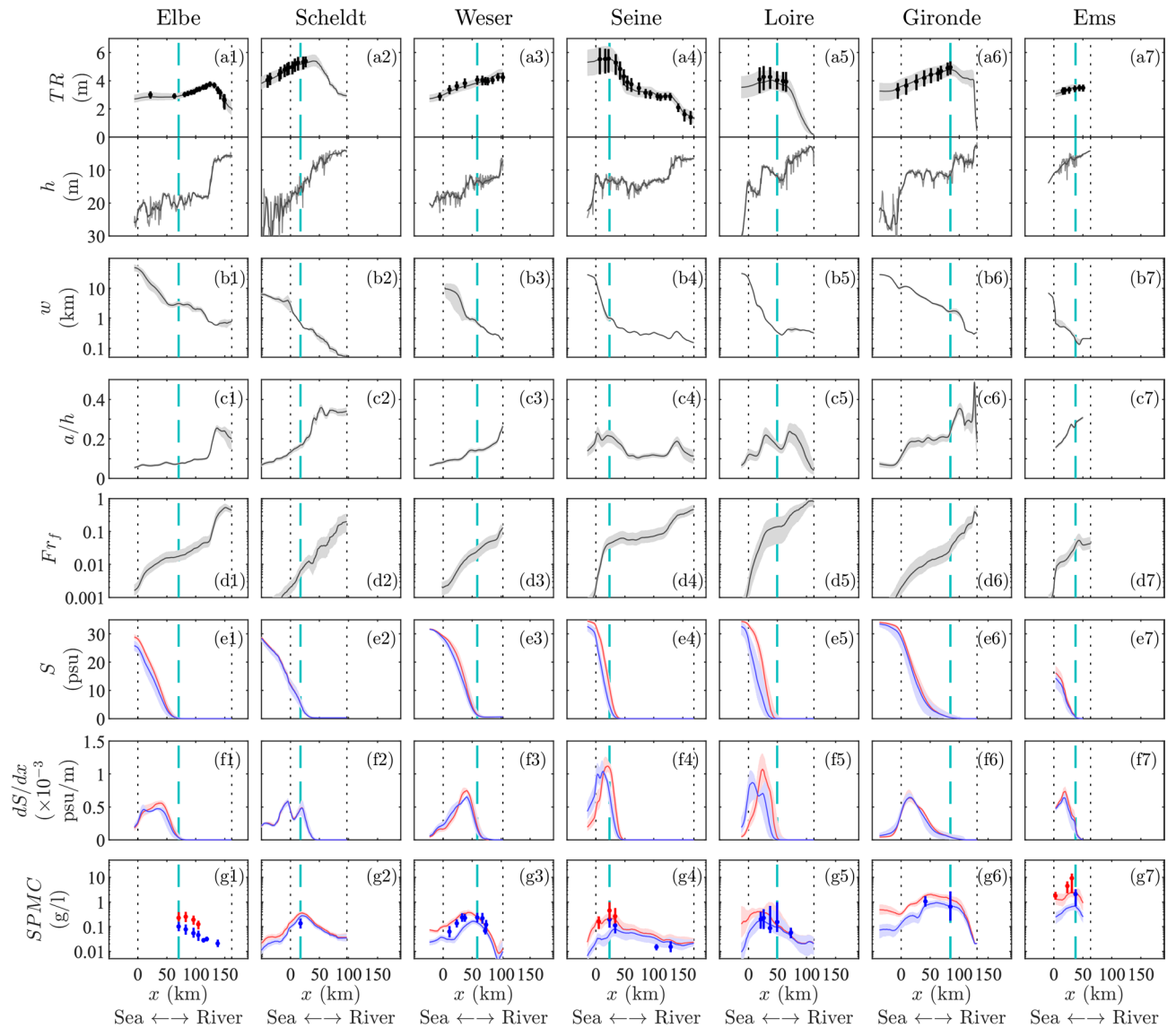


Fig. 2. Longitudinal transects of physical parameters in the seven main estuaries. **(a)** Tidal range TR and water depth h , **(b)** estuary width w , **(c)** relative tidal amplitude a/h , **(d)** freshwater Froude number Fr_f , **(e)** salinity S , **(f)** horizontal salinity gradient dS/dx , and **(g)** SPM concentration $SPMC$. One-year-averaged medians of simulated (lines) and measured (symbols) data. The shaded areas and error bars represent the 25th–75th percentile distributions of simulations and measurements, respectively. In panels (e to g), bottom and surface data are in red and blue, respectively. The cyan vertical dashed lines represent the yearly-averaged locations of maximum measured surface SPMC, and black vertical dotted lines represent yearly-averaged seaward and landward estuary boundaries. SPMC simulations were not available in the Elbe Estuary configuration.

energy systems^{59,60}. And fourthly, the present ETM distribution is derived from semidiurnal meso- to macro-tidal estuaries and relatively low river discharge conditions. As part of future work, our diagram could be complemented with a broader range of conditions⁴, such as diurnal tidal forcing, larger river systems with higher discharge and sediment loads, such as Asian river-delta systems and South American estuaries under the influence of the Amazon River plume^{61,62}.

A turbidity diagram for exploring the potential impacts of human pressures

The ETM parameter space can also be used to examine the impact of human-induced pressures on ETM within tide-dominated systems, such as estuary deepening^{63,64}. For example, the Loire Estuary in 1900 had a shallower navigation channel than it does today ($h_m = 5$ m instead of 9.3 m; Table 1), which was associated with lower SPMC^{13,15}. The shift from low- to hyper-turbid conditions during the 20th century is visible in the ETM parameter space, with $a_0/h_m - Fr_{s,m}$ values closer to the high-turbidity hotspot in 2000 than in 1900 (L_{19} and L_{20} in Fig. 3b). Therefore, the configuration of the Loire Estuary shifted from dispersive conditions to ones that favour sediment trapping. Although concurrent anthropogenic factors (e.g., sediment supply reduction,

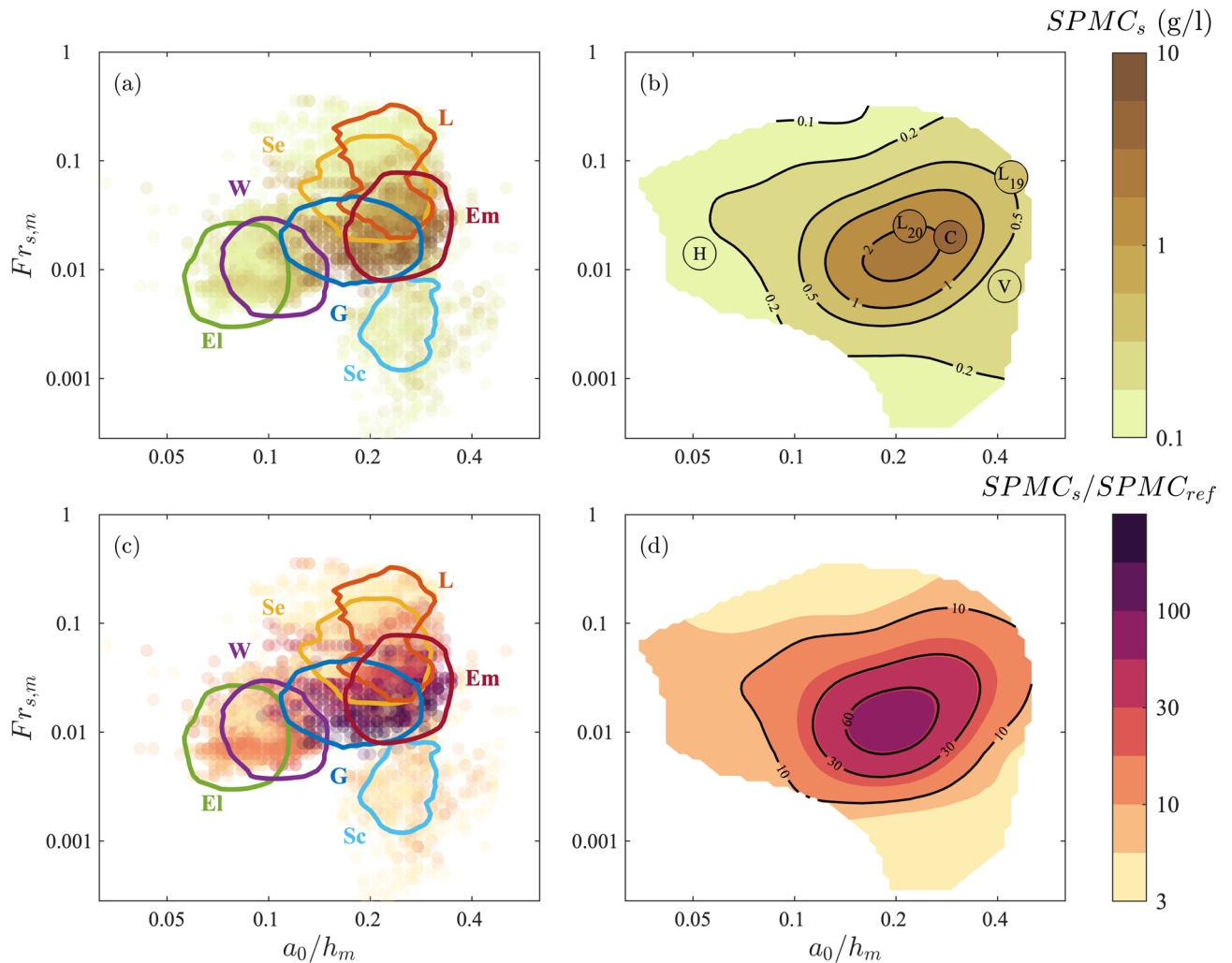


Fig. 3. Parameter space for estuarine turbidity maximum. **(a–b)** Highest quartile (75th percentile) of in-situ surface SPM concentration $SPMC_s$ and **(c–d)** estuarine trapping efficiency $SPMC_s/SPMC_{ref}$ based on the relative tidal amplitude a_0/h_m and simplified freshwater Froude number $Fr_{s,m}$. **(a, c)** Scatter plot of tide-averaged data for the seven main estuaries with the main occurrence area (coloured contours), and **(b, d)** interpolated data with black isolines. In panel **(b)**, open circles represent in-situ observations for the test estuaries using values defined in Table 1: ‘C’ Charente, ‘V’ Vilaine, ‘H’ Hudson, ‘L₁₉’ Loire in 1900, and ‘L₂₀’ Loire in 2000.

engineering works) may also have influenced the SPMC in the Loire Estuary during the 20th century, the current ETM diagram captures some of the change in state.

Deepening of the Ems Estuary has resulted in a substantial increase in SPMC^{14,64,65}. With a smaller water depth h_m , the a_0/h_m of the pristine Ems Estuary was likely higher than that of the present-day estuary, a region characterised by lower SPMC in Fig. 3. This example therefore supports the idea that the highest SPMC tends to be located in the centre of the a_0/h_m – $Fr_{s,m}$ diagram. In many estuaries, hydrodynamics are influenced not only by deepening but also by other human impacts, such as harbour extensions, dam construction, and estuary narrowing⁶⁶, which could also be explored using this approach. However, human activities that result in a significant decrease in sediment availability cannot be examined using the current ETM diagram (e.g., large-scale maintenance dredging activities, sediment removal).

Methods

Estuary boundary definition

Comparing different estuaries requires a consistent description of the systems and their boundaries. Many definitions of estuaries exist, such as those based on geological, tidal, salinity, or biological properties^{67,68}. In this study, we aim to characterise the active part of a tidal estuary in terms of physical functioning. The upward boundary is defined at the limit of tidal influence, when the relative tidal amplitude $a/h = 0$. This limit may correspond to locations where the tide is blocked by a weir (e.g., Seine Estuary) or fully dissipated (e.g., Loire Estuary). The seaward boundary is defined at the location where the local Froude number exceeds a threshold

value (here, 0.002). This value corresponds to situations where estuarine stratification begins to be significant^{29,46}. A value of 0.002 is slightly arbitrary, but a sensitivity test revealed that using 0.001 or 0.003 as a threshold does not significantly impact the results. The distance between the seaward and landward boundaries defines the along-channel estuary length, L_{est} (Fig. 1). The relative length is the ratio of the estuary length to the tidal wave length (L_{est}/L_{tide}), with $L_{tide} = \sqrt{g h_m} / \omega$ the tidal length, g the gravitational acceleration, ω the semidiurnal tidal frequency, and h_m the median depth along the estuary (Table 1).

Multi-estuary in-situ measurements and numerical simulations

Morphologies and forcing are based on one-year numerical simulations from previously published studies and validated against in-situ data (see the Data Availability section). We extracted longitudinal transects from the three-dimensional configurations along the estuary thalweg x ($x=0$ at the seaward boundary and increases landward; Fig. 2). This implies that the effects of lateral processes on the main channel dynamics are not specifically addressed, although their contributions are present in the extracted data. These simulations provided high-frequency (every 15–60 min) and high-resolution (every 100–500 m) information on water levels, current velocities, salinity, and SPMC distributions.

Additionally, one-year in-situ measurement datasets (Fig. 2; Table 1) are used to derive the ETM distribution in relation to the forcing parameters (i.e., tidal amplitude, river discharge, and morphology). To capture the highest turbidity levels, we selected data from the station measuring the largest SPMC along the estuary transect. Surface measurements were chosen because they are more frequently available in estuaries and provide a more accurate indication of the potential light attenuation within the water column. The high-frequency data (every 5–30 min) were processed using the highest quartile (i.e., the 75th percentile) of the surface SPMC ($SPMC_s$) per tidal cycle to represent the tide-averaged estuarine turbidity maximum.

To compute the estuarine trapping efficiency ($SPMC_s/SPMC_{ref}$), the dominant source of SPMC ($SPMC_{ref}$) is the river discharge for all the estuaries except for the Ems and the Weser, where a marine source is dominant. The fluvial- or marine-dominant sources were identified based on the literature review^{14,31,33,39,41,69–71}, and the values were extracted from the current study datasets at the estuary boundaries (see the Data Availability section). An exception was made for the Ems, which used the value from a larger scale analysis⁷² because the actual lower boundary did not extend sufficiently seaward.

Although interannual variability in river forcing affects SPM response in estuaries^{34,70,71,73}, the chosen years display enough fluctuations in river discharge to provide a representative view of ETM dynamics. However, note that extreme events, such as extremely high or low river discharges, may not be captured in the present study^{74,75}.

After establishing the ETM distribution based on the seven main estuaries, we completed our analysis by testing additional estuarine configurations (Table 1): (i) the short macro-tidal, low-turbid Vilaine Estuary (France); (ii) the medium-sized macro-tidal, hyper-turbid Charente Estuary (France); (iii) the long meso-tidal, low-turbid Hudson Estuary (USA); and (iv) a comparison of the Loire Estuary (France) in 1900 and 2000, when the channel depth was significantly deepened.

Simplified estuarine parameters

The parameter space for maximum SPMC is defined by two parameters that serve as proxies for the main drivers of ETM formation: baroclinic circulation and tidal asymmetry. The baroclinic circulation relates to the strength of the salinity gradient, which can be approximated with the freshwater Froude number Fr_f ⁴⁷. Fr_f represents the net velocity due to river flow scaled by the maximum possible frontal propagation speed⁷⁶:

$$Fr_f = U_R / (\beta g S_o h)^{\frac{1}{2}} \quad (1)$$

where $U_R = Q/A$ is the river velocity, with Q the river discharge and A the estuary cross-section area, S_o the ocean salinity, and $\beta = 7.7 \times 10^{-4}$ kg/g the haline contraction coefficient.

Estimating Fr_f from in-situ data is difficult because a representative estuary cross-section area is not easily determined in estuarine systems. We therefore develop a simplified expression for Fr_f , enabling straightforward exploration of the turbidity parameter space across a broader range of estuaries. The forcing variables herein are the river discharge at the landward (i.e., up-estuary) boundary Q_0 , the water depth along the estuary thalweg $h(x)$, and the estuary width $w(x)$, which can, for example, be obtained from satellite images. Therefore, the estuary cross-section can be approximated as $A_s = h \times w$. Note that using the estuary width at low tide (w_{lw}) better represents the main channel and improves the section area estimate. To derive an integrated parameter at the system scale, the simplified freshwater Froude number is given by

$$Fr_{s,m} = U_{Rs,m} / (\beta g S_o h_m)^{\frac{1}{2}} \text{ with } U_{Rs,m} = Q_0 / (h_m \cdot w_m) \quad (2)$$

where h_m and w_m are the along-estuary median of the thalweg mean water depth and low-water cross-section width, respectively. This simplification proved to be a very satisfactory estimate for Fr_f at the estuary scale (Figure S4).

Tidal asymmetries can be calculated using various methods to quantify dephasing in tidal components, which causes differences in the duration and/or magnitude of ebb and flood phases (for water elevation and current velocity)^{52,77–79}. Here, we use an approach based on tidal distortion, computed as the relative tidal amplitude (a/h)²⁸, the larger the tidal amplitude relative to the water depth, the larger its distortion by bed friction. This method provides less detailed information on tidal asymmetry characteristics than previous methods and, for example, cannot distinguish between flood- or ebb-dominance, which may lead to contrasting residual sediment transport⁸⁰. Here, we assume that the relative tidal amplitude indicates flood dominance, which is the most

commonly observed phenomenon^{28,77,79}. This straightforward formulation offers the advantage of a robust quantification of tidal deformation using easily obtainable estuarine parameters, thus making it applicable to a wider range of poorly documented systems.

Following the previously adopted strategy for the simplified Froude number, we quantify the tidal asymmetry integrated over the entire estuary domain as a_0/h_m , where a_0 is the tidal amplitude at the seaward boundary. Note that this parameter, integrated over the estuary system (per tidal cycle), does not account for changes in bed roughness and intertidal morphologies⁴⁷. This integrated approach can be viewed as considering an estuarine system like a “box”, characterised by a specific geometry (i.e., depth and width), and driven by a tidal forcing at the seaward boundary and a river discharge at the landward boundary.

Data availability

The in-situ measurement and numerical simulation datasets used in this study were collected from previously published works and open data sources for the Elbe, Scheldt, Weser, Seine, Loire (2018), Gironde, Ems, Vilaine, Charente, Loire (1900 and 2000), and Hudson estuaries. Elbe in-situ measurements from www.kuestendaten.de and Strotmann⁸¹, and numerical simulations from Reese, et al.³⁰. Scheldt in-situ measurements from *Flanders Hydraulics* and numerical simulations from van Kessel, et al.³¹ and Plancke, et al.⁸². Weser in-situ measurements retrieved by the *Federal Waterways and Shipping Administration*, provided by the *Federal Waterways Engineering and Research Institute*, and numerical simulations from the 3D hydrodynamic model of the Weser Estuary based on UnTRIM2, conducted and provided by the *Federal Waterways Engineering and Research Institute*³². Seine in-situ measurements from the SYNAPSES network^{83,84} and numerical simulations from Grasso, et al.⁸⁵ and Grasso, et al.⁶⁶. Loire in-situ measurements from the SYVEL network^{70,86} and numerical simulations from Grasso and Caillaud³⁴ and Grasso and Caillaud⁸⁷. Gironde in-situ measurements from the MAGEST network^{71,88} and numerical simulations from Diaz, et al.⁸⁹ and Diaz, et al.³⁵. Ems in-situ measurements from Lower Saxony Water Management, Coastal and Nature Protection Agency (NLWKN) and numerical simulations from van Maren, et al.¹⁴. Vilaine in-situ measurements from Traini, et al.¹⁶ and Vested, et al.⁴⁸. Charente in-situ measurements from Toublanc, et al.⁴⁹. Loire (1900 and 2000) in-situ measurements from Dijkstra and de Goede¹⁵. Hudson in-situ measurements from Geyer, et al.⁵⁰ and Warner, et al.⁹⁰.

Received: 10 September 2025; Accepted: 15 December 2025

Published online: 23 December 2025

References

1. Leuven, J. R., Pierik, H. J., van der Vegt, M., Bouma, T. J. & Kleinans, M. G. Sea-level-rise-induced threats depend on the size of tide-influenced estuaries worldwide. *Nat. Clim. Change*. **9**, 986–992 (2019).
2. Guo, L. et al. A historical review of sediment export–import shift in the North Branch of Changjiang Estuary. *Earth Surface Processes and Landforms* n/a <https://doi.org/10.1002/esp.5084> (2021).
3. Yang, S. L., Zhang, J. & Xu, X. Influence of the three Gorges dam on downstream delivery of sediment and its environmental implications, Yangtze river. *Geophysical Res. Lett.* **34** (2007).
4. Nienhuis, J. H. et al. Global-scale human impact on delta morphology has led to net land area gain. *Nature* **577**, 514–518 (2020).
5. Wei, X. et al. Nutrient transport and transformation in macrotidal estuaries of the French Atlantic coast: a modeling approach using the Carbon-Generic estuarine model. *Biogeosciences* **19**, 931–955 (2022).
6. Horemans, D. M., Meire, P. & Cox, T. J. The impact of Temporal variability in light-climate on time-averaged primary production and a phytoplankton bloom in a well-mixed estuary. *Ecol. Model.* **436**, 109287 (2020).
7. Abril, G. et al. A massive dissolved inorganic carbon release at spring tide in a highly turbid estuary. *Geophys. Res. Lett.* **31** (2004).
8. Cui, Y., Wu, J., Tan, E. & Kao, S. J. Role of particle resuspension in maintaining hypoxic level in the Pearl River Estuary. *Journal of Geophysical Research: Oceans* **127**, e2021JC018166 (2022).
9. Grasso, F., Carlier, A., Cugier, P., Verney, R. & Marzloff, M. Influence of crepidula fornicata on suspended particle dynamics in coastal systems: a mesocosm experimental study. *J. Ecohydraulics*. **8**, 26–37 (2023).
10. Wilber, D. H. & Clarke, D. G. Biological effects of suspended sediments: a review of suspended sediment impacts on fish and shellfish with relation to dredging activities in estuaries. *North Am. J. Fish. Manag.* **21**, 855–875 (2001).
11. Uncles, R., Stephens, J. & Smith, R. The dependence of estuarine turbidity on tidal intrusion length, tidal range and residence time. *Cont. Shelf Res.* **22**, 1835–1856 (2002).
12. Jay, D. A., Orton, P. M., Chisholm, T., Wilson, D. J. & Fain, A. M. V. Particle trapping in stratified estuaries: application to observations. *Estuaries Coasts*. **30**, 1106–1125 (2007).
13. Winterwerp, J. C., Wang, Z. B., van Braeckel, A., van Holland, G. & Kösters, F. Man-induced regime shifts in small estuaries—II: a comparison of rivers. *Ocean Dyn.* **63**, 1293–1306 (2013).
14. van Maren, D. S., Winterwerp, J. C. & Vroom, J. Fine sediment transport into the hyper-turbid lower Ems river: the role of channel deepening and sediment-induced drag reduction. *Ocean Dyn.* **65**, 589–605. <https://doi.org/10.1007/s10236-015-0821-2> (2015).
15. Dijkstra, Y. M. & de Goede, R. J. Regime shift to hyperturbid conditions in the Loire estuary: Overview of observations and model analysis of physical mechanisms. *J. Geophys. Res. Oceans* **129**, e2023JC020273 (2024).
16. Traini, C., Proust, J. N., Menier, D. & Mathew, M. Distinguishing natural evolution and human impact on estuarine morpho-sedimentary development: A case study from the Vilaine Estuary, France. *Estuar. Coast. Shelf Sci.* **163**, 143–155 (2015).
17. Figueroa, S. M. & Son, M. Transverse variability of residual currents, sediment fluxes, and bed level changes in estuaries with an estuarine dam: role of estuarine type, dam location, and discharge interval. *Cont. Shelf Res.* **274**, 105196 (2024).
18. Figueroa, S. M. & Son, M. Estuarine dams and weirs: global analysis and synthesis. *Mar. Geol.* **477**, 107388 (2024).
19. Kim, T., Choi, B. & Lee, S. Hydrodynamics and sedimentation induced by large-scale coastal developments in the keum river Estuary, Korea. *Estuar. Coast. Shelf Sci.* **68**, 515–528 (2006).
20. Scully, M. E. & Friedrichs, C. T. Sediment pumping by tidal asymmetry in a partially mixed estuary. *J. Geophys. Res. Oceans* **112** (2007).
21. Allen, G. P., Salomon, J., Bassoullet, P., Du Penhoat, Y. & De Grandpre, C. Effects of tides on mixing and suspended sediment transport in macrotidal estuaries. *Sed. Geol.* **26**, 69–90 (1980).
22. Talke, S. A., de Swart, H. E. & Schuttelaars, H. Feedback between residual circulations and sediment distribution in highly turbid estuaries: an analytical model. *Cont. Shelf Res.* **29**, 119–135 (2009).
23. Dronkers, J. Tide-Induced residual transport of fine sediment. *Phys. Shallow Estuaries Bays*, 228–244 (1986).
24. Jay, D. A. & Musiak, J. D. Particle trapping in estuarine turbidity maxima. *J. Phys. Res.* **99**, 446–420 (1994).

25. Burchard, H., Schuttelaars, H. M. & Ralston, D. K. Sediment trapping in estuaries. *Annual Rev. Mar. Sci.* **10**, 371–395 (2018).
26. Burchard, H. & Baumert, H. The formation of estuarine turbidity maxima due to density effects in the salt wedge. A hydrodynamic process study. *J. Phys. Oceanogr.* **28**, 309–321 (1998).
27. Druine, F. et al. In situ high frequency long term measurements of suspended sediment concentration in turbid estuarine system (Seine Estuary, France): optical turbidity sensors response to suspended sediment characteristics. *Mar. Geol.* **400**, 24–37 (2018).
28. Friedrichs, C. T. & Aubrey, D. G. Non-linear tidal distortion in shallow well-mixed estuaries: a synthesis. *Estuar. Coast. Shelf Sci.* **27**, 521–545 (1988).
29. Geyer, W. R. & MacCready, P. The estuarine circulation. *Annu. Rev. Fluid Mech.* **46**, 175–197. <https://doi.org/10.1146/annurev-fluid-010313-141302> (2014).
30. Reese, L. et al. Local mixing determines Spatial structure of diahaline exchange flow in a mesotidal estuary: A study of extreme runoff conditions. *J. Phys. Oceanogr.* **54**, 3–27 (2024).
31. van Kessel, T., vanlede, J. & de Kok, J. Development of a mud transport model for the Scheldt estuary. *Cont. Shelf Res.* **31**, S165–S181 (2011).
32. Kolb, P., Zorndt, A., Burchard, H., Gräwe, U. & Kösters, F. Modelling the impact of anthropogenic measures on saltwater intrusion in the Weser estuary. *Ocean Sci.* **18**, 1725–1739 (2022).
33. Grasso, F. et al. Suspended sediment dynamics in the macrotidal Seine estuary (France): 1. Numerical modeling of turbidity maximum dynamics. *J. Geophys. Research: Oceans.* **123**, 558–577. <https://doi.org/10.1002/2017JC013185> (2018).
34. Grasso, F. & Caillaud, M. A ten-year numerical hindcast of hydrodynamics and sediment dynamics in the Loire estuary. *Sci. Data.* **10**, 394 (2023).
35. Diaz, M., Grasso, F., Sottolichio, A., Le Hir, P. & Caillaud, M. Investigating sediment dynamics on a continental shelf mud patch under the influence of a macrotidal estuary: a numerical modeling analysis. *Contin. Shelf Res.* **105334** (2024).
36. Le Floch, J. Propagation de la marée dynamique dans l'estuaire de la Seine et la Seine Maritime. *Unpublished PhD dissertation, University of Paris, France* (1961).
37. Dalrymple, R. W. & Choi, K. Morphologic and facies trends through the fluvial–marine transition in tide-dominated depositional systems: a schematic framework for environmental and sequence-stratigraphic interpretation. *Earth Sci. Rev.* **81**, 135–174 (2007).
38. Winterwerp, J. C. & Wang, Z. B. Hydrosedimentological response to estuarine deepening: conceptual analysis. *J. Waterw. Port Coast. Ocean Eng.* **147**, 04021023 (2021).
39. Kappenberg, J. & Grabemann, I. Variability of the mixing zones and estuarine turbidity maxima in the Elbe and Weser estuaries. *Estuaries* **24**, 699–706 (2001).
40. van Gils, J., Ouboter, M. & De Rooij, N. Modelling of water and sediment quality in the Scheldt estuary. *Netherland J. Aquat. Ecol.* **27**, 257–265 (1993).
41. Grabemann, I. & Krause, G. On different time scales of suspended matter dynamics in the Weser estuary. *Estuaries* **24**, 688–698 (2001).
42. Avoine, J., Allen, G., Nichols, M., Salomon, J. & Larssonneur, C. Suspended-sediment transport in the Seine estuary, france: effect of man-made modifications on estuary—shelf sedimentology. *Mar. Geol.* **40**, 119–137 (1981).
43. Le Hir, P. & Thouvenin, B. Mathematical modelling of cohesive sediment and particulate contaminants transport in the Loire Estuary. *OLSEN & OLSEN, FREDENSBORG, DENMARK.*, 71–78 (1994).
44. Castaing, P. & Allen, G. P. Mechanisms controlling seaward escape of suspended sediment from the gironde: a macrotidal estuary in France. *Mar. Geol.* **40**, 101–118 (1981).
45. Winterwerp, J. C. Fine sediment transport by tidal asymmetry in the high-concentrated Ems river: indications for a regime shift in response to channel deepening. *Ocean Dyn.* **61**, 203–215 (2011).
46. MacCready, P. & Geyer, W. R. Advances in estuarine physics. *Annual Rev. Mar. Sci.* **2**, 35–58 (2010).
47. Valle-Levinson, A. *Contemporary Issues in Estuarine Physics* (Cambridge University Press, 2010).
48. Vested, H. J., Tessier, C., Christensen, B. B. & Goubert, E. Numerical modelling of morphodynamics—Vilaine estuary. *Ocean Dyn.* **63**, 423–446 (2013).
49. Toublanc, F., Brenon, I. & Coulombier, T. Formation and structure of the turbidity maximum in the macrotidal Charente estuary (France): influence of fluvial and tidal forcing. *Estuar. Coast. Shelf Sci.* **169**, 1–14. <https://doi.org/10.1016/j.ecss.2015.11.019> (2016).
50. Geyer, W. R., Woodruff, J. & Traykovski, P. Sediment transport and trapping in the Hudson river estuary. *Estuaries* **24**, 670–679 (2001).
51. Ralston, D. K. & Geyer, W. R. Response to channel deepening of the salinity intrusion, estuarine circulation, and stratification in an urbanized estuary. *J. Geophys. Research: Oceans.* **124**, 4784–4802 (2019).
52. Nidzieski, N. & Ralston, D. Tidal asymmetry and velocity skew over tidal flats and shallow channels within a macrotidal river delta. *J. Geophys. Res. Oceans* **117** (2012).
53. Friedrichs, C. T., Armbrust, B. D. & De Swart, H. E. Hydrodynamics and equilibrium sediment dynamics of shallow, funnel-shaped tidal estuaries. *Phys. Estuaries Coastal. Seas*, 315–327 (1998).
54. Uncles, R., Elliott, R. & Weston, S. Dispersion of salt and suspended sediment in a partly mixed estuary. *Estuaries* **8**, 256–269 (1985).
55. Deloffre, J. et al. Controlling factors of rhythmic sedimentation processes on an intertidal estuarine mudflat—role of the turbidity maximum in the macrotidal Seine estuary, France. *Mar. Geol.* **235**, 151–164 (2006).
56. McSweeney, J. M., Chant, R. J. & Sommerfield, C. K. Lateral variability of sediment transport in the D Delaware E Stuary. *J. Geophys. Research: Oceans.* **121**, 725–744 (2016).
57. Verney, R., Lafite, R. & Brun-Cottan, J. C. Flocculation potential of estuarine particles: the importance of environmental factors and of the Spatial and seasonal variability of suspended particulate matter. *Estuaries Coasts.* **32**, 678–693 (2009).
58. Winterwerp, J. On the flocculation and settling velocity of estuarine mud. *Cont. Shelf Res.* **22**, 1339–1360 (2002).
59. Green, M. O. & Coco, G. Review of wave-driven sediment resuspension and transport in estuaries. *Rev. Geophys.* **52**, 77–117. <https://doi.org/10.1002/2013rg000437> (2014).
60. Chen, L. et al. Axial wind effects on stratification and longitudinal sediment transport in a convergent estuary during wet season. *J. Geophys. Research: Oceans.* **125**, e2019JC015254 (2020).
61. Abascal-Zorrilla, N. et al. Dynamics of the estuarine turbidity maximum zone from landsat-8 data: the case of the Maroni river Estuary, French Guiana. *Remote Sens.* **12**, 2173 (2020).
62. van Maren, D. S. & Hoekstra, P. Seasonal variation of hydrodynamics and sediment dynamics in a shallow subtropical estuary: the Ba Lat River, Vietnam. *Estuar. Coast. Shelf Sci.* **60**, 529–540. <https://doi.org/10.1016/j.ecss.2004.02.011> (2004).
63. Grasso, F. & Le Hir, P. Influence of morphological changes on suspended sediment dynamics in a macrotidal estuary: diachronic analysis in the Seine estuary (France) from 1960 to 2010. *Ocean Dyn.* **69**, 83–100 (2019).
64. de Jonge, V. N., Schuttelaars, H. M., van Beusekom, J. E., Talke, S. A. & de Swart, H. E. The influence of channel deepening on estuarine turbidity levels and dynamics, as exemplified by the Ems estuary. *Estuar. Coast. Shelf Sci.* **139**, 46–59 (2014).
65. Dijkstra, Y. M., Schuttelaars, H. M., Schramkowski, G. P. & Brouwer, R. L. Modeling the transition to high sediment concentrations as a response to channel deepening in the Ems river estuary. *J. Geophys. Research: Oceans.* **124**, 1578–1594 (2019).
66. Grasso, F., Bismuth, E. & Verney, R. Unraveling the impacts of meteorological and anthropogenic changes on sediment fluxes along an estuary-sea continuum. *Sci. Rep.* **11**, 1–11 (2021).
67. Dalrymple, R. W., Zaitlin, B. A. & Boyd, R. Estuarine facies models: conceptual basis and stratigraphic implications: perspective. *J. Sediment. Res.* **62** (1992).

68. Elliott, M. & McLusky, D. S. The need for definitions in Understanding estuaries. *Estuar. Coast. Shelf Sci.* **55**, 815–827 (2002).
69. Kappenberg, J. et al. Seasonal, spring-neap and tidal variation of hydrodynamics and water constituents in the mouth of the Elbe estuary, Germany. *Ocean Sci. Discuss.*, 1–31 (2016).
70. Jalón-Rojas, I., Schmidt, S., Sottolichio, A. & Bertier, C. Tracking the turbidity maximum zone in the Loire estuary (France) based on a long-term, high-resolution and high-frequency monitoring network. *Cont. Shelf Res.* **117**, 1–11. <https://doi.org/10.1016/j.csr.2016.01.017> (2016).
71. Jalón-Rojas, I., Schmidt, S. & Sottolichio, A. Turbidity in the fluvial Gironde estuary (southwest France) based on 10-year continuous monitoring: sensitivity to hydrological conditions. *HESS* **19**, 2805–2819. <https://doi.org/10.5194/hess-19-2805-2015> (2015).
72. van Maren, D. S. & Cronin, K. Uncertainty in complex three-dimensional sediment transport models: equifinality in a model application of the Ems Estuary, the Netherlands. *Ocean Dyn.* **66**, 1665–1679. <https://doi.org/10.1007/s10236-016-1000-9> (2016).
73. Coynel, A. et al. Sampling frequency and accuracy of SPM flux estimates in two contrasted drainage basins. *Sci. Total Environ.* **330**, 233–247 (2004).
74. Poppeschi, C., Verney, R. & Charria, G. Suspended particulate matter response to extreme forcings in the Bay of Seine. *Mar. Geol.* **472**, 107292 (2024).
75. Ralston, D. K., Yellen, B., Woodruff, J. D. & Fernald, S. Turbidity hysteresis in an estuary and tidal river following an extreme discharge event. *Geophys. Res. Lett.* **47**, e2020GL088005 (2020).
76. Geyer, W. R. Estuarine salinity structure and circulation. *Contemp. Issues Estuar. Phys.*, 12–26 (2010).
77. Nidzieski, N. J. Tidal asymmetry in estuaries with mixed semidiurnal/diurnal tides. *J. Geophys. Res. Oceans* **115** (2010).
78. Van Maren, D. & Gerritsen, H. Residual flow and tidal asymmetry in the Singapore Strait, with implications for resuspension and residual transport of sediment. *J. Geophys. Res. Oceans* **117** (2012).
79. Hoitink, A., Hoekstra, P. & Van Maren, D. Flow asymmetry associated with astronomical tides: implications for the residual transport of sediment. *J. Geophys. Res. Oceans* **108** (2003).
80. Guo, L., Van der Wegen, M., Roelvink, J. & He, Q. The role of river flow and tidal asymmetry on 1-D estuarine morphodynamics. *J. Geophys. Research: Earth Surf.* **119**, 2315–2334 (2014).
81. Strotmann, T. Deutsches Gewässerkundliches Jahrbuch: Elbegebiet, Teil III: Untere Elbe ab der Havelmündung, *Freie und Hansestadt Hamburg, HPA Hamburg Port Authority*, 179 pp., (2013). https://dgi.de/docs/eiii_2013.pdf (2015).
82. Plancke, Y. et al. The sand and mud budget of the Zeeschelde since the start of the twenty-first century. *J. Soils Sediments*, 1–15 (2024).
83. Druine, F. Flux sédimentaires en estuaire de Seine: Quantification et variabilité multi-échelle sur la base de mesures de turbidité (réseau SYNAPSES). *Thèse de Doctorat, Université de Rouen Normandie* (2018).
84. GIP Seine-Aval & GPM Rouen. <http://www.seine-aval.fr/reseau-synapses/>
85. Grasso, F., Bismuth, E., Verney, R. & CurviSeine Hindcast IFREMER. (2019). <https://doi.org/10.12770/8f5ec053-52c8-4120-b031-4e4b6168ff29>
86. GIP Loire Estuaire. <http://www.loire-estuaire.org/dif/do/init>
87. Grasso, F., Caillaud, M. & CurviLoire Hindcast IFREMER. (2023). <https://doi.org/10.12770/a56f1a01-bdf2-4f52-9cc7-4e4b8605520c>
88. Schmidt, S., Etcheber, H., Sottolichio, A. & Castaing, P. Bilan de 10 ans de suivi haute-fréquence de la qualité des eaux de l'estuaire de la Gironde. *system* **97**, 98 (2016).
89. Diaz, M., Grasso, F., Caillaud, M. & CurviGironde Hindcast IFREMER. (2023). <https://doi.org/10.12770/44ac4d72-c606-42ba-bf22-89e6520e0894>
90. Warner, J. C., Geyer, W. R. & Lerczak, J. A. Numerical modeling of an estuary: A comprehensive skill assessment. *J. Geophys. Res. Oceans* **110** (2005).

Acknowledgements

This work was conducted within the framework of the CAPTURE project funded by the French Agency for Biodiversity (OFB) under the Mission Inter-Estuaire (MIE) program. The authors acknowledge Yoeri Dijkstra, Henk Schuttelaars, Rocky Geyer, Romaric Verney, Stefan Talke, and Steven Figueroa for their valuable and constructive comments on the manuscript.

Author contributions

The study analysis was jointly conducted by all the authors. F.G. proposed the main idea for the study and performed the supervision. In situ data and numerical simulations were provided by H.B., F.G., L.R., T.K., J.V., D.S.M., A.Z., and compiled by E.B. F.G. led the visualisation of the results and the writing of the paper, to which all co-authors contributed.

Funding

E.B., F.G., and S.D. received funding from the Agency for Biodiversity (OFB) under the Mission Inter-Estuaire (MIE) programme.

Declarations

Competing interests

The authors declare no competing interests

Additional information

Supplementary Information The online version contains supplementary material available at <https://doi.org/10.1038/s41598-025-32950-7>.

Correspondence and requests for materials should be addressed to F.G.

Reprints and permissions information is available at www.nature.com/reprints.

Publisher's note Springer Nature remains neutral with regard to jurisdictional claims in published maps and institutional affiliations.

Open Access This article is licensed under a Creative Commons Attribution-NonCommercial-NoDerivatives 4.0 International License, which permits any non-commercial use, sharing, distribution and reproduction in any medium or format, as long as you give appropriate credit to the original author(s) and the source, provide a link to the Creative Commons licence, and indicate if you modified the licensed material. You do not have permission under this licence to share adapted material derived from this article or parts of it. The images or other third party material in this article are included in the article's Creative Commons licence, unless indicated otherwise in a credit line to the material. If material is not included in the article's Creative Commons licence and your intended use is not permitted by statutory regulation or exceeds the permitted use, you will need to obtain permission directly from the copyright holder. To view a copy of this licence, visit <http://creativecommons.org/licenses/by-nc-nd/4.0/>.

© The Author(s) 2025